Title

ECG and navigator-free four-dimensional whole-heart coronary MRA for simultaneous visualization of cardiac anatomy and function

Journal

Magnetic Resonance in Medicine, 72(5)

ISSN

0740-3194

Authors

Pang, Jianing
Sharif, Behzad
Fan, Zhaoyang
et al.

Publication Date

2014-11-01

DOI

10.1002/mrm.25450

Peer reviewed

Published in final edited form as:
Magn Reson Med. 2014 November ; 72(5): 1208–1217. doi:10.1002/mrm.25450.

ECG and Navigator-Free 4D Whole-Heart Coronary MRA for Simultaneous Visualization of Cardiac Anatomy and Function

Jianing Pang[1,2], **Behzad Sharif**[2], **Zhaoyang Fan**[2], **Xiaoming Bi**[3], **Reza Arsanjani**[2], **Daniel S. Berman**[2], and **Debiao Li**[2,4]

[1]Department of Radiology and Biomedical Engineering, Northwestern University, Chicago, Illinois, USA

[2]Biomedical Imaging Research Institute, Cedars-Sinai Medical Center, Los Angeles, California, USA

[3]MR R&D, Siemens Healthcare, Los Angeles, California, USA

[4]University of California, Los Angeles, California, USA

Abstract

Purpose—To develop a cardiac and respiratory self-gated 4D coronary MRA technique for simultaneous cardiac anatomy and function visualization.

Methods—A contrast-enhanced, ungated spoiled gradient echo sequence with self-gating (SG) and 3DPR trajectory was used for image acquisition. Data was retrospectively binned into different cardiac and respiratory phases based on information extracted from SG projections using principal component analysis. Each cardiac phase was reconstructed using a respiratory motion-corrected self-calibrating SENSE framework, and those belong to the quiescent period were retrospectively combined for coronary visualization. Healthy volunteer studies were conducted to evaluate the efficacy of the SG method, the accuracy of the left ventricle (LV) function parameters and the quality of coronary artery visualization.

Results—SG performed reliably for all subjects including one with poor ECG. The LV function parameters showed excellent agreement with those from a conventional cine protocol. For coronary imaging, the proposed method yielded comparable apparent SNR and coronary sharpness and lower apparent CNR on three subjects compared with an ECG and navigator-gated Cartesian protocol and an ECG-gated, respiratory motion-corrected 3DPR protocol.

Conclusion—A fully self-gated 4D whole-heart imaging technique was developed, potentially allowing cardiac anatomy and function assessment from a single measurement.

Keywords

coronary MRA; cine imaging; self-gating; 3D radial acquisition

Correspondence to: Debiao Li, Ph.D., Biomedical Imaging Research Institute, Cedars-Sinai Medical Center, 8700 Beverly Blvd, PACT Suite 800, Los Angeles, CA, USA 90048, Phone: 310-423-7743, debiao.li@cshs.org.

INTRODUCTION

Motion artifact suppression is a major challenge in coronary magnetic resonance angiography (MRA). Cardiac motion is usually addressed by prospective electrocardiogram (ECG) gating, in which the data acquisition window is placed within the most quiescent cardiac phase, usually in mid-diastole, with a predetermined duration and delay after the R-wave trigger (1,2). For respiratory motion, the typical method is prospective navigator gating, in which a k-space segment is repeatedly acquired until the corresponding diaphragm position, tracked by a navigator, falls within a predetermined range in the superior-inferior (SI) direction (3).

These approaches bear a number of limitations. In prospective ECG gating, the fixed trigger delay and acquisition window duration, determined visually from a cine pre-scan, are not only reader-dependent but can also become invalid should the heart rate of the subject changes significantly. Furthermore, the ECG waveform can be distorted and yield incorrect triggers due to chest deformity or the magnetohydrodynamic effect (4). Last, setting up the ECG electrodes can be time-consuming and require operator expertise. Likewise, issues such as vulnerability to respiratory pattern drifts, operator dependency, reduced scan efficiency, as well as extra setup time, are also present in respiratory navigator gating.

An alternative approach to address cardiac motion is retrospective ECG gating, commonly used in cardiac cine imaging. The k-space data is acquired continuously and then resorted into different cardiac phases during reconstruction based on the simultaneously recorded ECG information (5,6). In this way, the entire cardiac cycle can be visualized. However, the continuous acquisition precludes conventional free-breathing techniques such as navigator gating, and usually relies on breath-holding for respiratory motion suppression. As a result, the total scan time is restricted to 10–15 sec, limiting the spatiotemporal resolution and spatial coverage. A number of strategies have been proposed to enable free-breathing, including real-time imaging and respiratory self-gating. Real-time imaging resolves both cardiac and respiratory motion by achieving high temporal resolution through various acceleration techniques, albeit at a cost of spatial resolution and coverage (7–9). Respiratory self-gating (SG) allows free-breathing acquisition by extracting motion information from imaging data (10). This information can then be used for retrospective respiratory gating or respiratory motion corrected averaging (11,12). Free of the scan time constraint, a larger spatial coverage may be achieved (13,14). Breath-hold cardiac SG (15,16) and simultaneous cardiac and respiratory SG (14,17,18) have also been proposed to further eliminate the need to obtain ECG signal.

A number of previous works have proposed continuous acquisition strategies for coronary MRA allowing the user to retrospectively select the time window for optimal coronary visualization (19–24). The cardiac phase information is obtained by either concurrently recorded ECG signal (19–23) or cardiac SG (24), and the required fat-suppressed bright-blood contrast was achieved using balanced steady-state free precession (bSSFP) readout and phase-sensitive fat-suppression (19,21,22), interleaved fat-suppression modules (23), spoiled gradient echo readout with T1-shortening contrast agent (20), or fat-water separation with a multi-echo bSSFP readout (24). Achieved spatial coverage ranges from targeted thin

slab with non-isotropic spatial resolution (19–22,24) to isotropic whole-heart (23). Most utilize view sharing to reconstruct different cardiac phases (19,20,23,24). Reported scan times are 20–24 sec (19,20), 4–6 min (21,22,24) and 14 min (23). Methods for respiratory motion suppression include breath-holding (19,20) and respiratory SG (21–24).

In this work, we proposed an improved 4D coronary MRA technique with free-breathing acquisition, simultaneous cardiac and respiratory self-gating and isotropic whole-heart coverage that allowed cardiac anatomy and function assessment from a single measurement. First, we developed and validated a simultaneous cardiac and respiratory SG method based on SI projections and principal component analysis (PCA). Second, we extended our previous 3DPR based motion correction and sensitivity-encoding framework (25–27) to enable cardiac phase-resolved reconstruction with 100% respiratory gating efficiency. Then, we evaluated the accuracy of the left ventricle (LV) function parameters derived from the proposed method by comparing against conventional breath-hold cine protocols. Last, we performed preliminary comparisons between the proposed technique and two prospectively ECG gated coronary MRA protocols in terms of apparent signal-to-noise ratio (aSNR), apparent contrast-to-noise ratio (aCNR) and coronary sharpness.

METHODS

Extraction of Cardiac and Respiratory Motion Signals

In this work, we achieved simultaneous cardiac and respiratory SG through SI readouts inserted at regular intervals during imaging. After Fourier transform, the resulting image space projection profiles were organized as the following (N_c×N_r)-by-N_{SG} matrix:

$$A=\begin{bmatrix} U_1 \\ \vdots \\ U_{N_c} \end{bmatrix}, \text{with} U_\gamma=\begin{bmatrix} u_\gamma(x_1,t_1) & \dots & u_\gamma(x_1,t_{N_{SG}}) \\ \vdots & \ddots & \vdots \\ u_\gamma(x_{N_r},t_1) & \dots & u_\gamma(x_{N_r},t_{N_{SG}}) \end{bmatrix} \text{for} \gamma=1,2,\dots N_c$$

where N_c is the number of coils, N_r is the number of readout points, and N_{SG} is the total number of SG lines. Considering the imaging volume was repeatedly projected onto the same SI axis, the variations in the projection profiles through time should be largely attributed to the underlying cardiac and respiratory motion. Treating each stacked multi-coil projection profile as a single point in an N_c×N_r dimensional measurement space, we hypothesize that the motion signals lie along the principal components found by PCA (18). To determine if a principal component represented cardiac or respiratory motion, its major Fourier mode was identified, and if the frequency matched typical cardiac (0.75–2.0 Hz, 45–120 bpm) or respiratory (0.1–0.5 Hz) ranges, it would be assigned as the cardiac or respiratory component. This procedure began with the first principal component and was repeated on the following ones until both cardiac and respiratory motion signals were identified. Then, each k-space line was assigned its respective cardiac and respiratory phases according to the motion signals, essential for the subsequent respiratory motion correction, detailed in the following sections.

Cardiac SG Processing and Sampling Rate Requirement

The cardiac SG triggers were located using simple valley detection. Then, each imaging line can be mapped to the respective cardiac phase based on its relative position between two triggers. Intuitively, the SG lines needed to be played out frequently enough to correctly capture the cardiac motion. According to the Nyquist-Shannon sampling theorem, a band-limited signal can be perfectly sampled at a rate twice its bandwidth. However, due to heart rate variation, the cardiac motion is not band-limited, and therefore the Nyquist rate formula is not directly applicable. To empirically determine the required oversampling factor on healthy volunteers (compared to the Nyquist rate specified by the average heart rate), we performed the following study. First, a 25-heartbeat-long dataset consisting of only SI projections was acquired on a healthy subject. Then, the SG time series was downsampled temporally, and the accordance between cardiac SG and ECG triggers was measured in terms of the standard deviation of the differences in SG and ECG trigger times. This step was repeated until there was significant error in the SG triggering times.

Respiratory SG Processing and Motion Correction

We hypothesized that the respiratory PCA component was correlated to the SI translation found by the cross-correlation based template matching method used in previous works (26–28), and the k-space data can be allocated into different respiratory phases accordingly. To test this hypothesis, we calculated the correlation of the respiratory PCA component and the SI translation found by template matching (26,27) for each subject.

After cardiac and respiratory binning, the heartbeats with duration more than two standard deviations away from the mean were discarded. Also, the outlier respiratory positions, defined as those more than two standard deviations away from the mean respiratory position, were binned into the outermost respiratory bin. Then, a previously developed image-based framework was adapted for respiratory motion correction (26,27). The k-space data was assigned to 54 bins spanning 9 cardiac and 6 respiratory phases, such that both types of motion were adequately resolved and, at the same time, each bin contained at least 1,000 lines for reconstructing an acceptable 3D image by gridding with appropriate low-pass filtering. One of the respiratory phases, usually in end-expiration, was identified as the reference phase. Then, separately for each cardiac phase, the remaining bins were registered to the corresponding reference bins using an affine transform model. The resulting transform parameters were subsequently used to modify k-space data and trajectory for respiratory motion correction. The workflow is summarized in Fig. 1. Additional figures showing the effect of motion correction can be viewed in online supplementary material.

Dual-Mode Image Reconstruction

A self-calibrating sensitivity encoding framework was used for image reconstruction to suppress the streaking artifacts from radial undersampling (27). Given the total amount of data available, the major tradeoff in 4D reconstruction was between cardiac motion-resolving performance (number of cardiac phases) and image quality (number of lines per phase). After respiratory motion correction, the data may be divided into an arbitrary number of cardiac frames thanks to the sampling pattern stability offered by the golden means-based 3D radial trajectory (29). Using all k-space data, a “performance-driven” 16-

phase reconstruction was first performed to visualize cardiac motion and derive functional parameters such as end systolic volume (ESV), end diastolic volume (EDV) and ejection fraction (EF) (30). No data was shared between adjacent phases. Then, the quiescent period, which may contain more than one of the 16 cardiac phases, was visually identified to and the corresponding k-space data was combined to yield a “quality-driven” reconstruction intended for coronary visualization.

In Vivo Experiment

In vivo studies were performed on nine healthy volunteers (three men, average age 38.6±13.4 years) with IRB approval and written consent obtained before the scan. MR data was collected using a clinical 3T scanner (MAGNETOM Verio, Siemens Healthcare, Erlangen, Germany) with a 32-channel receiver coil array.

After initial localization, 2D breath-hold bSSFP cine protocol was performed at 10–12 short-axis locations covering the entire LV with the following parameters: TR/TE = 2.9/1.3 ms, flip angle = 50°, readout bandwidth = 1313 Hz/pixel, FOV = 320×240 mm^2, matrix size = 224×168, slice thickness = 8 mm, slice gap = 2 mm, retrospective ECG gating, number of reconstructed cardiac phases = 25. Total scan time was 10–15 min including the rest time between the breath-holds.

Next, 4D data was collected during free breathing using an ungated spoiled gradient echo pulse sequence: 1-2-1 water selective hard pulse, TR/TE = 5.5/3.0 ms, flip angle = 15°, bandwidth = 449 Hz/pixel, FOV = 400^3 mm^3, matrix size = 384^3, total number lines = 109,000, scan time = 10 min regardless of the heart rate or breathing pattern of the subject. To improve blood-myocardium contrast, a 0.20 mmol/kg Gd-BOPTA (MultiHance, Bracco Imaging SpA, Milano, Italy) bolus was injected at 3.0 ml/s prior to image acquisition. For the 16-phase reconstruction, each phase had a temporal footprint of 62.5 ms (assuming 60 bpm heart rate) and contained approximately 6,800 lines which, suggested by our previous work, provided adequate image quality (27). ECG signal was recorded from the scanner physiological measurement unit for comparison purposes.

Furthermore, three subjects underwent two additional coronary scans on separate visits. First, an ECG and diaphragm navigator-gated, fat-suppressed, inversion recovery (IR) prepared, spoiled gradient echo sequence with 3D Cartesian trajectory: TR/TE = 3.4/1.5 ms, flip angle = 20°, inversion time = 200 ms, bandwidth = 710 Hz/pixel, FOV = 320×250×96 mm^3, matrix size = 320×250×96, GRAPPA factor = 2, slice partial Fourier factor = 7/8, 5 mm navigator acceptance window. Second, an ECG-gated, fat-suppressed, IR prepared spoiled gradient echo sequence with spiral-on-sphere 3DPR k-space trajectory (31): TR/TE = 3.5/1.8 ms, flip angle = 18°, inversion time = 300 ms, bandwidth = 704 Hz/pixel, FOV = 400^3 mm^3, matrix size = 384^3, number of projections = 12,000, free-breathing with retrospective self-navigated respiratory motion correction (26,27). Both scans were performed with 0.20 mmol/kg Gd-BOPTA enhancement, and the data acquisition window was set to the cardiac quiescent period as determined from a four-chamber cine pre-scan.

For the radial acquisitions, the image reconstruction was implemented offline using MATLAB (Mathworks, Natick, MA) with parallel computing toolbox on a workstation with

12-core Intel Xeon CPU and 96 GB memory. To reduce the memory requirement, channel compression was performed using the method proposed by Buehrer et al (32). The processing time was around 120 min for motion correction, and around 60 min per cardiac phase for the non-Cartesian SENSE image reconstruction. The images were reformatted using OsiriX (v5.8.5 32-bit, Pixmeo, Geneva, Switzerland) and CoronaViz (Siemens Corporate Research, Princeton, NJ).

Data Analysis

First, we examined the accuracy of cardiac and respiratory SG for each subject. We calculated the standard deviation of the difference between SG and ECG trigger times as a measure of SG trigger accuracy. We also calculated the correlation between respiratory SG component and the SI translation curve derived by template matching.

Next, we examined the agreement of the ESV, EDV and EF values measured from 2D cine and the 16-phase 4D image series using linear regression and Bland-Altman analysis. The multiple short-axis locations of the 2D cine series were retrospectively found in the 4D series. For each slice location, the LV area was calculated from the manually traced blood-myocardium boundary. For statistical analysis, we used paired Student's t-test with the *P*-value threshold set at 0.05.

Then, we compared the quiescent phase reconstruction with the ECG and navigator-gated Cartesian coronary MRA protocol (Cartesian) and the ECG-gated 3DPR coronary MRA protocol (ECG+3DPR). The numbers of projections in the proposed method and ECG +3DPR were matched. Image quality was evaluated in terms of aSNR, aCNR and coronary sharpness. The aSNR and aCNR were calculated from the mean signal intensities in the blood pool and myocardium regions-of-interest (ROIs) and, to partially address the spatially varying noise distribution due to parallel imaging, the signal standard deviation in the same blood pool ROI as the apparent noise level. The ROI locations were matched among different scans for the same subject. The coronary sharpness was measured using the method proposed in (33) at proximal locations of left main and right coronary arteries and compared on a per-vessel basis.

RESULTS

SG Sampling Rate Requirement

Fig. 2a shows the cardiac SG component of the example subject with different sampling rates and the reference ECG waveform plotted against a common time axis. The vertical lines and the circles indicate ECG R-wave triggers and SG triggers, respectively. For this subject, SG triggering performed reliably with sampling rates as low as 4.0 Hz, approximately 4 times the heart rate (around 60 bpm). Lower SG sampling rates led to unreliable trigger times or even missed triggers. This observation was confirmed by a quantitative analysis on the SG trigger uncertainty, measured by the standard deviation (SD) of the difference between SG and ECG trigger times. Shown in Fig. 2b, the uncertainty remained low until 3.0 Hz and drastically increases at 2.8 Hz. SG sampling rates lower than 2.8 Hz resulted in missing triggers and the SD was not calculated.

In all subsequent in vivo studies, we used a SG sampling rate of 12 Hz 15-line imaging segment), which was expected to be robust for the normal range of heart rates.

Performance of Cardiac and Respiratory SG in Healthy Subjects

Cardiac SG performed reliably on all subjects, including one (subject 8) who showed poor ECG signal despite multiple attempts to place the electrodes. Excluding this subject, the average SD value of the difference between SG and ECG trigger times was 30.9 ± 2.8 ms. The average correlation between respiratory principal component and the SI translations derived from cross-correlation-based template matching was 0.95 ± 0.02.

Shown in Fig. 3 are (a) cardiac PCA component, (b) ECG waveform, (c) respiratory PCA component, (d) respiratory SI translation by template matching, and (e) the SG projection time series from one channel for subject 8. The cardiac PCA component displayed distinct triggering features, whereas the ECG signal yielded incorrect triggers. The sagittal scout image (f) of this subject showed a chest deformity that likely compromised the ECG signal reception. The conventional ECG-triggered cine protocol (g) showed significant blurring due to incorrect cardiac triggering. Running the same protocol using pulse triggering (h) improved the image quality. The four-chamber reformat of the self-gated 4D series (i) showed excellent image quality.

Left Ventricle Function Parameters

For eight out of the nine subjects (excluding subject 8), ESV, EDV and EF values were calculated from the breath-hold 2D and the 4D image series. As shown in Fig. 4, the LV function parameters obtained from the two methods showed good correlation. No statistically significant differences were found (ESV: $P = 0.10$, EDV: $P = 0.94$, EF: $P = 0.17$). The Bland-Altman analysis showed good agreement between the two measurement methods.

Quiescent Window Selection for Coronary Visualization

The heart rates of the nine subjects ranged from 51 to 86 bpm. The mean cardiac cycle durations and the identified quiescent periods are summarized in Fig. 5a. Cardiac phases that may be combined for coronary visualization are highlighted. In subjects with lower heart rates (subject 1–5, 9; 51–71 bpm), the quiescent window was in mid-diastole. However, for subjects with higher heart rates (subject 6–8; 76–86 bpm), the peak systole phase showed the least coronary motion. The durations of the quiescent phase ranged from 44 ms (systole, subject 7) to 283 ms (diastole, subject 9). For these two subjects, the reformatted four-chamber view of the 4D series are shown in Fig.5b and 5c, respectively.

Fig. 6 shows four reformatted quiescent phase reconstructions. The major coronary branches including LAD, LCX and RCA were clearly depicted. Additional 4D volumetric rendering and fly-through movies of one subject can be viewed in online supplementary material.

Comparing with Prospectively ECG Gated Protocols

While the scan time for the proposed 4D protocol was a fixed 10 min, the mean scan time for the ECG+3DPR protocol was 6.4±1.1 min, and the mean scan time for the Cartesian

protocol was 15.7±5.3 min with mean navigator efficiency of 35%±12%. For proposed, ECG+3DPR and Cartesian, the mean coronary sharpness were 0.35±0.08, 0.36±0.10 and 0.41±0.06, respectively; the mean aSNR were 12.4±3.8, 12.8±1.1 and 12.9±2.5, respectively, and the mean aCNR were 4.5±1.5, 6.8±0.3, and 10.2±3.0, respectively. The numbers are summarized in Fig. 7. Example images using the three protocols are shown in Fig. 8 for two subjects.

Also notable is that the specific absorption rate (SAR) of the proposed technique was well within limit (15%) and lower than that of ECG+3DPR (50%) due to the lack of inversion pulses. No complaints about the acoustic noise level were received from the subjects, though we did notice that the proposed sequence was somewhat louder than the conventional protocol due to the continuous rapid gradient switching.

DISCUSSION

In this proof-of-concept study, we developed an ECG and navigator-free 4D cardiac imaging technique with fixed 10-min free-breathing scan time, isotropic whole-heart coverage, as well as a flexible framework for retrospectively reconstructing any arbitrary cardiac phase.

The cardiac phase-resolved visualization from the proposed technique allowed volumetric cardiac function assessment. We compared the LV function parameters derived from the 4D image series with those from the conventional 2D cine protocol, and found excellent agreement between the two. Compared with previously proposed free-breathing 3D cine techniques (13,14), the proposed method offered considerable improvements in spatial coverage and resolution, ECG-free retrospective cardiac gating, as well as 100% acquisition efficiency through respiratory motion correction.

Furthermore, the proposed method delivered excellent visualization of the coronary anatomy in healthy subjects with a wide range of heart rates due to its high spatial resolution, whole-heart coverage and the flexibility of retrospective quiescent period selection. Within the paradigm of coronary MRA techniques with 100% acquisition efficiency (25,26,28,34–41), the proposed method presented a major technical development towards robust cardiac phase-resolved coronary imaging.

From the point of view of an end-user, the proposed method also provides several benefits. First, avoiding the potentially time-consuming ECG electrode placement procedure will considerably simplify the patient setup routine. Moreover, the ungated volumetric acquisition is essentially “push-button” as it only requires basic three-plane localization, reducing both the exam duration and setup complexity. Last, the proposed simultaneous cardiac and respiratory SG method was shown to have performed reliably in the healthy subjects scanned in this study, including one that displayed poor ECG signal. Therefore, the proposed technique may be more favorable under the situations where ECG triggering is unreliable.

Comparing with Prospectively ECG Gated Protocols

The proposed method differed from conventional coronary MRA techniques primarily in the cardiac gating strategy. Using the ECG signal as an external surrogate for cardiac motion, the conventional techniques prospectively synchronize data acquisition to the quiescent phase. Meanwhile, the dead time during the unacquired cardiac phases is used to play out the IR module, which imposes a heavy T1-weighting that essentially nulls the myocardial tissue. The proposed method, on the other hand, acquired data continuously and then retrospectively sorted the k-space lines into different cardiac phases. The blood-myocardium contrast thus relied on the steady-state T1 weighting which, in practice, cannot suppress the myocardial signal completely. This observation was corroborated by the preliminary healthy volunteer results where the aCNR of the proposed technique was lower than those of the two ECG-gated protocols with IR preparation. Whether this difference in blood-myocardium contrast will impact the detection of coronary stenosis, however, will require further systematic studies on CAD patients that benchmark the proposed technique with both the conventional coronary MRA protocol and x-ray angiography.

Beyond Steady-State Acquisition

In the proposed method, the fat-suppressed bright-blood image contrast, required to visualize the coronary arteries, was achieved in steady-state imaging using water-excitation RF pulses and T1-shortening contrast agent. However, it is possible to interleave magnetization preparation (mag-prep) modules with the imaging lines for contrast generation, such as fat-saturation modules in coronary imaging using bSSFP (23,42), as long as the cardiac SG remains reliable. Our preliminary analysis showed that the SI direction needed to be sampled at no less than 4 times the heart rate for cardiac SG to perform correctly. Assuming a maximum normal heart rate of 120 bpm, the maximum available interval between two SG lines will be 125 ms, which needs to accommodate both the mag-prep module and the imaging lines.

Dealing with Arrhythmia

The proposed technique enabled retrospective arrhythmia rejection by discarding the outlier heartbeats during reconstruction. For healthy subjects with regular sinus rhythm, the irregular heartbeats are infrequent and will not significantly affect the overall scan efficiency. Yet, for certain types of arrhythmia such as premature atrial and ventricular contraction (PAC and PVC), the premature beats may represent a significant portion of the scan time. In this case, both types of cardiac cycles may be reconstructed and visualized separately from the same dataset. The imaging time may have to be extended to accommodate a larger number of cardiac phases to be reconstructed. Further validation of the proposed cardiac SG method is also required in the presence of PAC, PVC and other types of arrhythmia, such as atrial fibrillation. Considering the higher degree of heart rate variation, the SG sampling rate requirement may also have to be revised.

Further Improving the Reconstruction

The tradeoff between cardiac phase-resolving performance and image quality was fundamental in the proposed reconstruction framework. Dividing the data into more cardiac

phases reduces residual cardiac motion in each phase, but leads to more aggressive undersampling and reduced image quality. To alleviate this constraint, it may be beneficial to exploit the spatiotemporal correlation in the multi-channel dataset (43–48). The improved image quality can then be traded to increase the temporal resolution or shorten the overall scan time. Also, considering that the current implementation took around 19 hours in total for motion correction, 16-phase cine reconstruction and the quiescent phase reconstruction, future efforts to shorten the reconstruction time are highly desirable in order to make the proposed technique more clinically feasible.

CONCLUSION

In this proof-of-concept study, we developed an ECG and navigator-free 4D whole-heart imaging technique with high isotropic spatial resolution and near 100% imaging efficiency through continuous acquisition, self-gating, retrospective respiratory motion correction and cardiac phase-resolved reconstruction. The proposed method potentially allows simultaneous cardiac anatomy and function assessment from a single measurement. Future efforts will be focused on optimization of both image acquisition and reconstruction, further validation of the obtained functional and anatomical information, as well as developing alternative, especially non-contrast acquisition strategies.

Supplementary Material

Refer to Web version on PubMed Central for supplementary material.

Acknowledgments

The authors thank Edward Gill, Lawrence St. John and Laura Smith for performing the conventional cine and coronary MRA protocols, Kimberly Okamoto for subject preparation, and Christy Woo for volunteer recruitment.

This project was supported in part by NIH grant numbers HL38698 and EB002623 (PI: Debiao Li, PhD), and American Heart Association Scientist Development Grant 14SDG20480123 (PI: Behzad Sharif, PhD).

REFERENCES

1. Wang Y, Vidan E, Bergman GW. Cardiac motion of coronary arteries: variability in the rest period and implications for coronary MR angiography. Radiology. 1999; 213:751–758. [PubMed: 10580949]
2. Wang Y, Watts R, Mitchell I, Nguyen TD, Bezanson JW, Bergman GW, Prince MR. Coronary MR angiography: selection of acquisition window of minimal cardiac motion with electrocardiography-triggered navigator cardiac motion prescanning--initial results. Radiology. 2001; 218:580–585. [PubMed: 11161182]
3. Danias PG, McConnell MV, Khasgiwala VC, Chuang ML, Edelman RR, Manning WJ. Prospective navigator correction of image position for coronary MR angiography. Radiology. 1997; 203:733–736. [PubMed: 9169696]
4. Keltner JR, Roos MS, Brakeman PR, Budinger TF. Magnetohydrodynamics of blood flow. Magn Reson Med. 1990; 16:139–149. [PubMed: 2255234]
5. Feinstein JA, Epstein FH, Arai AE, Foo TK, Hartley MR, Balaban RS, Wolff SD. Using cardiac phase to order reconstruction (CAPTOR): a method to improve diastolic images. J Magn Reson Imaging. 1997; 7:794–798. [PubMed: 9307903]

6. Carr JC, Simonetti O, Bundy J, Li D, Pereles S, Finn JP. Cine MR angiography of the heart with segmented true fast imaging with steady-state precession. Radiology. 2001; 219:828–834. [PubMed: 11376278]
7. Weiger M, Pruessmann KP, Boesiger P. Cardiac real-time imaging using SENSE. SENSitivity Encoding scheme. Magn Reson Med. 2000; 43:177–184. [PubMed: 10680680]
8. Nayak KS, Cunningham CH, Santos JM, Pauly JM. Real-time cardiac MRI at 3 tesla. Magn Reson Med. 2004; 51:655–660. [PubMed: 15065236]
9. Uecker M, Zhang S, Voit D, Karaus A, Merboldt KD, Frahm J. Real-time MRI at a resolution of 20 ms. NMR Biomed. 2010; 23:986–994. [PubMed: 20799371]
10. Larson AC, Kellman P, Arai A, Hirsch GA, McVeigh E, Li D, Simonetti OP. Preliminary investigation of respiratory self-gating for free-breathing segmented cine MRI. Magn Reson Med. 2005; 53:159–168. [PubMed: 15690515]
11. Kellman P, Chefd'hotel C, Lorenz CH, Mancini C, Arai AE, McVeigh ER. Fully automatic, retrospective enhancement of real-time acquired cardiac cine MR images using image-based navigators and respiratory motion-corrected averaging. Magn Reson Med. 2008; 59:771–778. [PubMed: 18302227]
12. Kellman P, Chefd'hotel C, Lorenz CH, Mancini C, Arai AE, McVeigh ER. High spatial and temporal resolution cardiac cine MRI from retrospective reconstruction of data acquired in real time using motion correction and resorting. Magn Reson Med. 2009; 62:1557–1564. [PubMed: 19780155]
13. Uribe S, Muthurangu V, Boubertakh R, Schaeffter T, Razavi R, Hill DL, Hansen MS. Whole-heart cine MRI using real-time respiratory self-gating. Magn Reson Med. 2007; 57:606–613. [PubMed: 17326164]
14. Liu J, Spincemaille P, Codella NC, Nguyen TD, Prince MR, Wang Y. Respiratory and cardiac self-gated free-breathing cardiac CINE imaging with multiecho 3D hybrid radial SSFP acquisition. Magn Reson Med. 2010; 63:1230–1237. [PubMed: 20432294]
15. Crowe ME, Larson AC, Zhang Q, Carr J, White RD, Li D, Simonetti OP. Automated rectilinear self-gated cardiac cine imaging. Magn Reson Med. 2004; 52:782–788. [PubMed: 15389958]
16. Larson AC, White RD, Laub G, McVeigh ER, Li D, Simonetti OP. Self-gated cardiac cine MRI. Magn Reson Med. 2004; 51:93–102. [PubMed: 14705049]
17. Buehrer M, Curcic J, Boesiger P, Kozerke S. Prospective self-gating for simultaneous compensation of cardiac and respiratory motion. Magn Reson Med. 2008; 60:683–690. [PubMed: 18727084]
18. Odille F, Uribe S, Batchelor PG, Prieto C, Schaeffter T, Atkinson D. Model-based reconstruction for cardiac cine MRI without ECG or breath holding. Magn Reson Med. 2010; 63:1247–1257. [PubMed: 20432296]
19. Park J, Larson AC, Zhang Q, Simonetti O, Li D. 4D radial coronary artery imaging within a single breath-hold: cine angiography with phase-sensitive fat suppression (CAPS). Magn Reson Med. 2005; 54:833–840. [PubMed: 16149060]
20. Bi X, Park J, Larson AC, Zhang Q, Simonetti O, Li D. Contrast-enhanced 4D radial coronary artery imaging at 3.0 T within a single breath-hold. Magn Reson Med. 2005; 54:470–475. [PubMed: 16032681]
21. Lai P, Huang F, Larson AC, Li D. Fast four-dimensional coronary MR angiography with k-t GRAPPA. J Magn Reson Imaging. 2008; 27:659–665. [PubMed: 18224671]
22. Lai P, Larson AC, Park J, Carr JC, Li D. Respiratory self-gated four-dimensional coronary MR angiography: a feasibility study. Magn Reson Med. 2008; 59:1378–1385. [PubMed: 18506786]
23. Coppo S, Piccini D, Chaptinel J, Bonanno G, Stuber M. Dynamic self-navigated 3D whole-heart radial coronary MRA with retrospective acquisition window selection. Journal of Cardiovascular Magnetic Resonance. 2014; 16:O18.
24. Liu J, Nguyen TD, Zhu Y, Spincemaille P, Prince MR, Weinsaft JW, Saloner D, Wang Y. Self-gated free-breathing 3D coronary CINE imaging with simultaneous water and fat visualization. PLoS One. 2014; 9:e89315. [PubMed: 24586682]
25. Bhat H, Ge L, Nielles-Vallespin S, Zuehlsdorff S, Li D. 3D radial sampling and 3D affine transform-based respiratory motion correction technique for free-breathing whole-heart coronary

MRA with 100% imaging efficiency. Magn Reson Med. 2011; 65:1269–1277. [PubMed: 21500255]

26. Pang J, Bhat H, Sharif B, Fan Z, Thomson LE, LaBounty T, Friedman JD, Min J, Berman DS, Li D. Whole-heart coronary MRA with 100% respiratory gating efficiency: self-navigated three-dimensional retrospective image-based motion correction (TRIM). Magn Reson Med. 2014; 71:67–74. [PubMed: 23401157]
27. Pang J, Sharif B, Arsanjani R, Bi X, Fan Z, Yang Q, Li K, Berman DS, Li D. Accelerated whole-heart coronary MRA using motion-corrected sensitivity encoding with three-dimensional projection reconstruction. Magn Reson Med.
28. Piccini D, Littmann A, Nielles-Vallespin S, Zenge MO. Respiratory self-navigation for whole-heart bright-blood coronary MRI: methods for robust isolation and automatic segmentation of the blood pool. Magn Reson Med. 2012; 68:571–579. [PubMed: 22213169]
29. Chan RW, Ramsay EA, Cunningham CH, Plewes DB. Temporal stability of adaptive 3D radial MRI using multidimensional golden means. Magn Reson Med. 2009; 61:354–363. [PubMed: 19165897]
30. Foo TK, Bernstein MA, Aisen AM, Hernandez RJ, Collick BD, Bernstein T. Improved ejection fraction and flow velocity estimates with use of view sharing and uniform repetition time excitation with fast cardiac techniques. Radiology. 1995; 195:471–478. [PubMed: 7724769]
31. Pang J, Yang Q, Li K, He Y, Fan Z, Sun B, Raman FS, Ahlman MA, Bluemke D, Bi X. High-resolution whole-heart contrast-enhanced coronary MRA in 5 minutes with self-navigation and 100% gating efficiency. Journal of Cardiovascular Magnetic Resonance. 2014; 16:O80.
32. Buehrer M, Pruessmann KP, Boesiger P, Kozerke S. Array compression for MRI with large coil arrays. Magn Reson Med. 2007; 57:1131–1139. [PubMed: 17534913]
33. Li D, Carr JC, Shea SM, Zheng J, Deshpande VS, Wielopolski PA, Finn JP. Coronary arteries: magnetization-prepared contrast-enhanced three-dimensional volume-targeted breath-hold MR angiography. Radiology. 2001; 219:270–277. [PubMed: 11274569]
34. Stehning C, Bornert P, Nehrke K, Eggers H, Stuber M. Free-breathing whole-heart coronary MRA with 3D radial SSFP and self-navigated image reconstruction. Magn Reson Med. 2005; 54:476–480. [PubMed: 16032682]
35. Moghari MH, Roujol S, Henningsson M, Kissinger KV, Annese D, Nezafat R, Manning WJ, Geva T, Powell AJ. Three-dimensional heart locator for whole-heart coronary magnetic resonance angiography. Magn Reson Med. 2014; 71:2118–2126. [PubMed: 23878103]
36. Henningsson M, Smink J, Razavi R, Botnar RM. Prospective respiratory motion correction for coronary MR angiography using a 2D image navigator. Magn Reson Med. 2013; 69:486–494. [PubMed: 22529009]
37. Henningsson M, Prieto C, Chiribiri A, Vaillant G, Razavi R, Botnar RM. Whole-heart coronary MRA with 3D affine motion correction using 3D image-based navigation. Magn Reson Med. 2014; 71:173–181. [PubMed: 23400902]
38. Prieto C, Doneva M, Usman M, Henningsson M, Greil G, Schaeffter T, Botnar RM. Highly efficient respiratory motion compensated free-breathing coronary mra using golden-step Cartesian acquisition. J Magn Reson Imaging.
39. Lai P, Bi X, Jerecic R, Li D. A respiratory self-gating technique with 3D-translation compensation for free-breathing whole-heart coronary MRA. Magn Reson Med. 2009; 62:731–738. [PubMed: 19526514]
40. Ingle RR, Wu HH, Addy NO, Cheng JY, Yang PC, Hu BS, Nishimura DG. Nonrigid autofocus motion correction for coronary MR angiography with a 3D cones trajectory. Magn Reson Med. 72:347–361. [PubMed: 24006292]
41. Wu HH, Gurney PT, Hu BS, Nishimura DG, McConnell MV. Free-breathing multiphase whole-heart coronary MR angiography using image-based navigators and three-dimensional cones imaging. Magn Reson Med. 2013; 69:1083–1093. [PubMed: 22648856]
42. Scheffler K, Heid O, Hennig J. Magnetization preparation during the steady state: fat-saturated 3D TrueFISP. Magn Reson Med. 2001; 45:1075–1080. [PubMed: 11378886]

43. Tsao J, Boesiger P, Pruessmann KP. k-t BLAST and k-t SENSE: dynamic MRI with high frame rate exploiting spatiotemporal correlations. Magn Reson Med. 2003; 50:1031–1042. [PubMed: 14587014]
44. Jung H, Ye JC, Kim EY. Improved k-t BLAST and k-t SENSE using FOCUSS. Phys Med Biol. 2007; 52:3201–3226. [PubMed: 17505098]
45. Kim D, Dyvorne HA, Otazo R, Feng L, Sodickson DK, Lee VS. Accelerated phase-contrast cine MRI using k-t SPARSE-SENSE. Magn Reson Med. 2012; 67:1054–1064. [PubMed: 22083998]
46. Hansen MS, Baltes C, Tsao J, Kozerke S, Pruessmann KP, Eggers H. k-t BLAST reconstruction from non-Cartesian k-t space sampling. Magn Reson Med. 2006; 55:85–91. [PubMed: 16323167]
47. Sharif B, Derbyshire JA, Faranesh AZ, Bresler Y. Patient-adaptive reconstruction and acquisition in dynamic imaging with sensitivity encoding (PARADISE). Magn Reson Med. 2010; 64:501–513. [PubMed: 20665794]
48. Sharif B, Bresler Y. Affine-corrected PARADISE: Free-breathing patient-adaptive cardiac MRI with sensitivity encoding. IEEE. 2007:1076–1079.

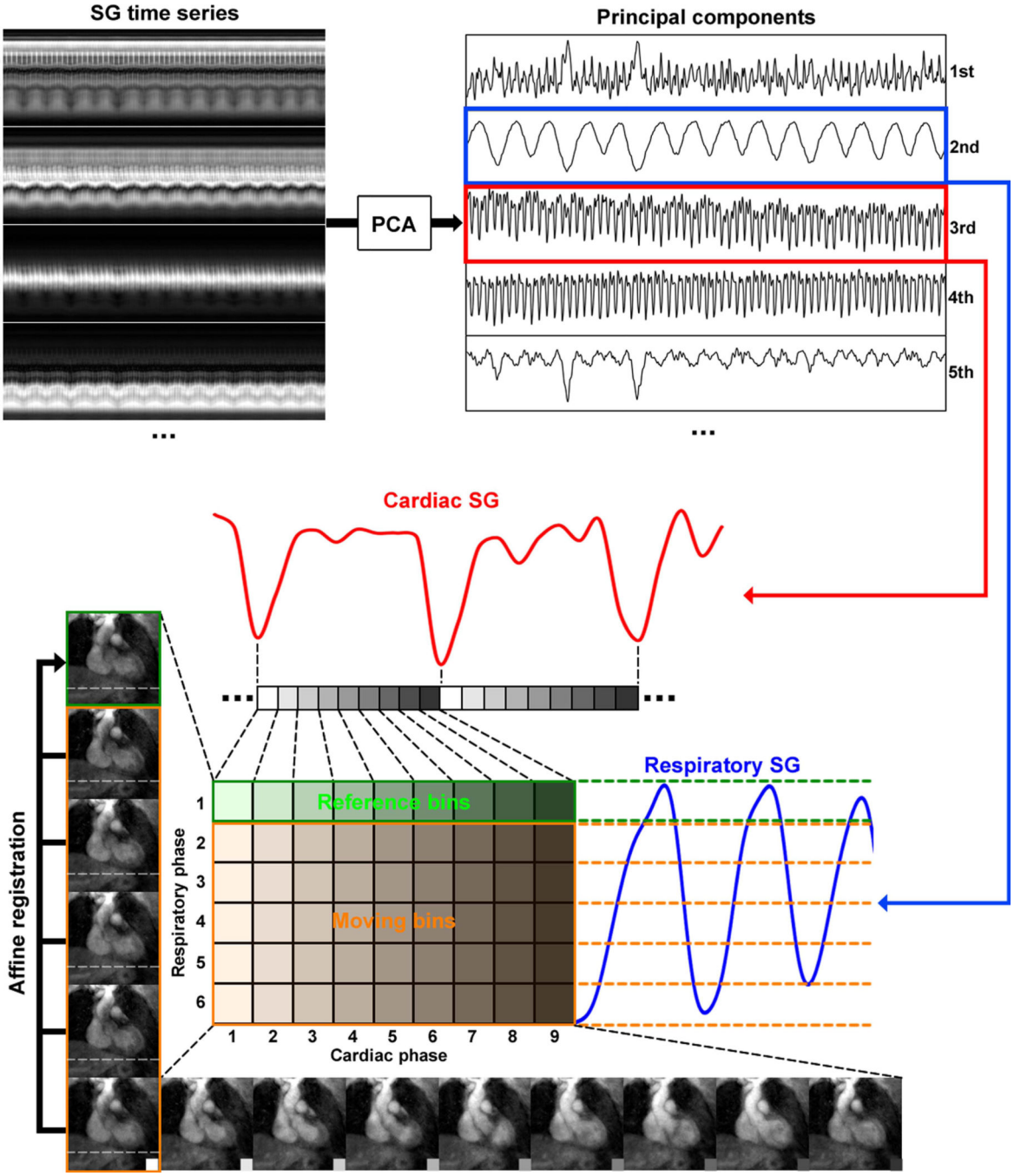

Figure 1.

Schematics of the proposed self-gating, data binning and respiratory motion correction framework. First, the cardiac and respiratory motion components were identified from the PCA of the multi-channel self-gating profile time series. Then, the imaging data was mapped to different cardiac and respiratory bins based on its cardiac and respiratory phase derived from the motion signals. Next, with one common respiratory phase selected as reference (in this example, respiratory phase 1 for cardiac phases 1–9), all other bins (respiratory phases 2–6, cardiac phases 1–9) were registered to the corresponding reference

bin of the same cardiac phase using an affine transform model. The k-space trajectory and data was then modified accordingly for respiratory motion correction. The 6 images on the left show the 6 respiratory phases in cardiac phase 1. The horizontal dashed lines help visualize the SI motion of the heart due to respiration. The 9 images on the bottom show the 9 cardiac phases in respiratory phase 6. The contraction of the left ventricle can be clearly seen.

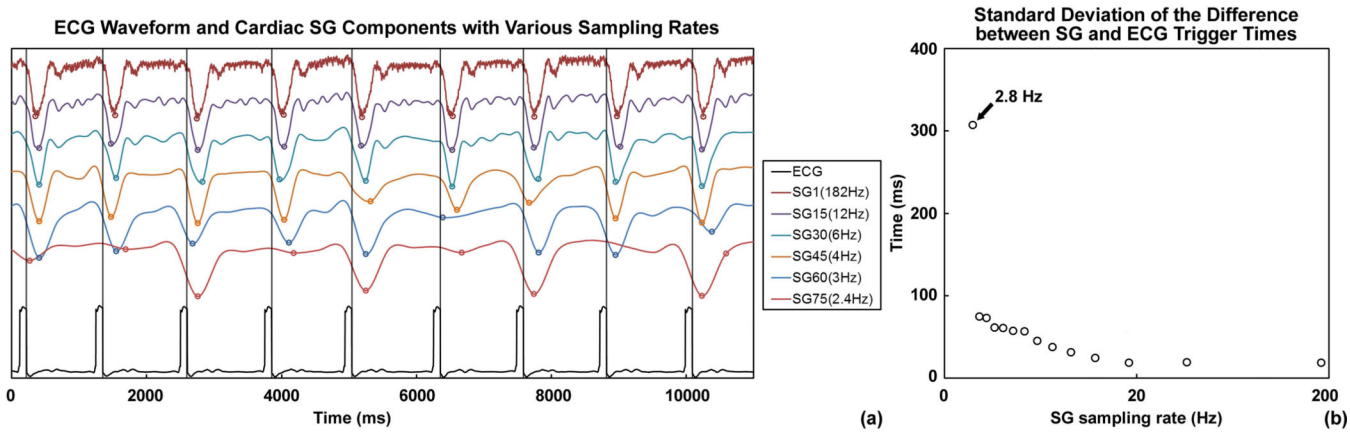

Figure 2.

(a) Cardiac principal components at different sampling rates with the reference ECG waveform, displayed on a common time axis. The vertical lines indicate the ECG R-wave triggers, and the circles on the SG waveform indicate the SG trigger times from valley detection. Comparing the two, cardiac SG performed reliably for sampling rates as low as 4.0 Hz. Lower rates led to inaccuracy in trigger times and missed trigger, as indicated by the two cardiac SG waveforms sampled at 3.0 Hz and lower. (b) The uncertainty in the SG trigger times was measured by the standard deviation (SD) of the difference between SG and ECG trigger times. The SD value remained low for sampling rates above 3.0 Hz and drastically increased at 2.8 Hz. Lower sampling rates resulted in missing triggers, thus the SD was not calculated.

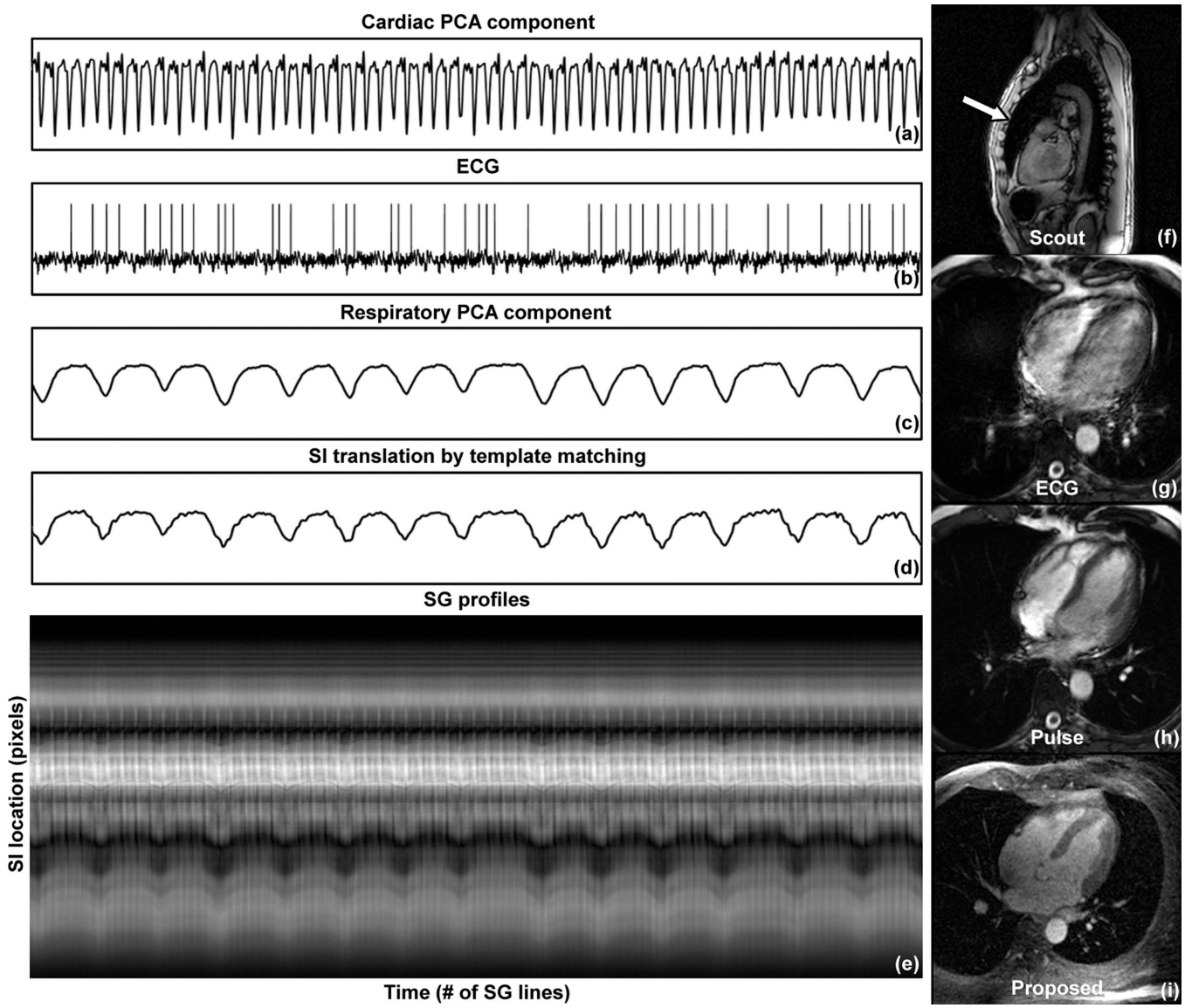

Figure 3.

A case of failed ECG triggering (subject 8). (a) Cardiac component; (b) ECG waveform; (c) Respiratory component; (d) SI translation detected by template matching; (e) SG projection time series. The cardiac SG waveform showed distinct valleys as triggering features. The ECG waveform yielded incorrect triggers, likely caused by the chest deformity shown in the sagittal scout image (f). The ECG triggered cine image showed significant blurring due to the unresolved cardiac motion (g). Switching to pulse triggering improved the image quality (h). The same four-chamber view was reformatted from the self-gated 4D series, showing excellent image quality (i).

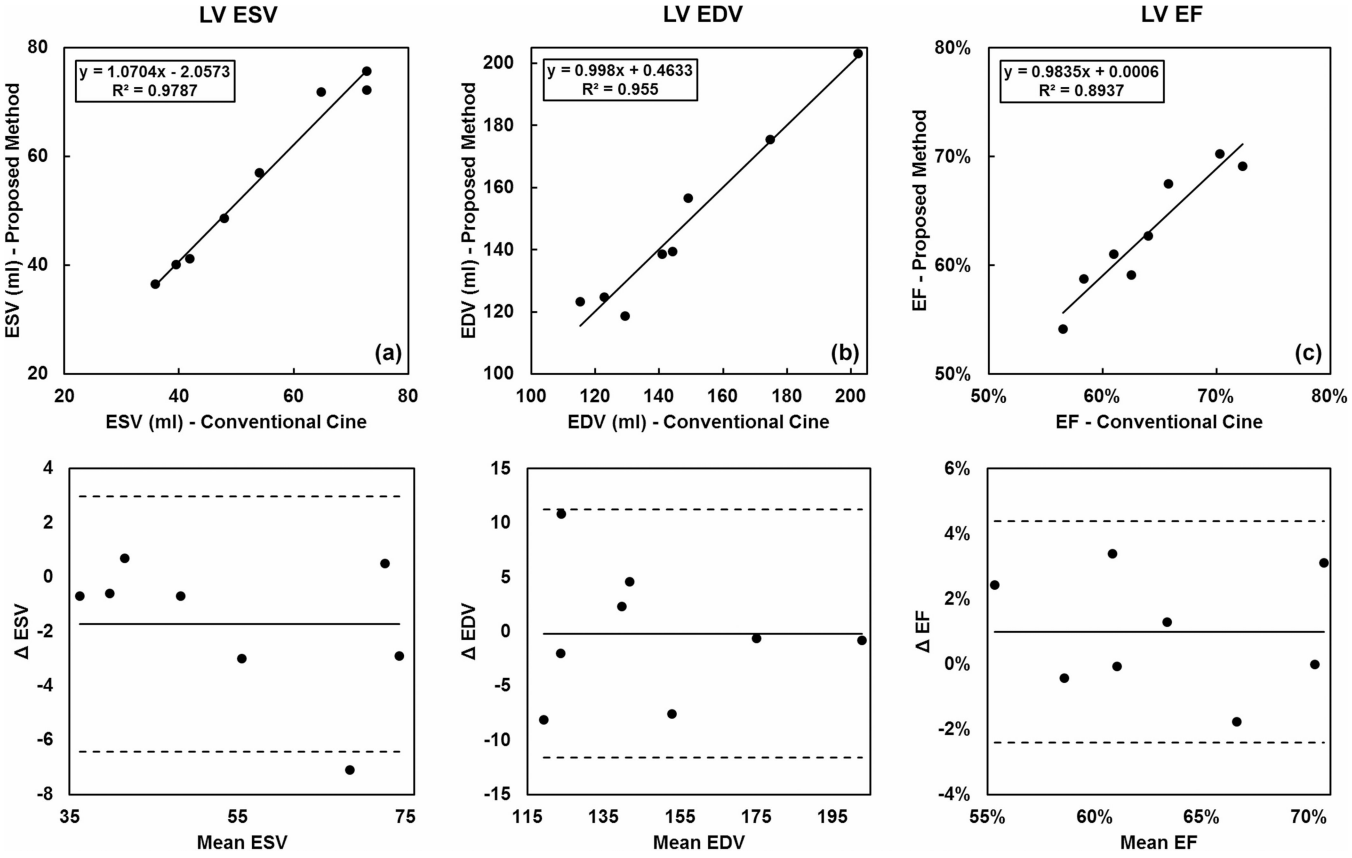

Figure 4.

Comparison of the left ventricle (LV) end-systolic volume (ESV), end-diastolic volume (EDV) and ejection fraction (EF) derived from both breath-hold 2D cine images and the proposed 4D technique. Good correlation and agreement were found between the two methods, as shown in the regression (a–c) and Bland-Altman analysis (d–f).

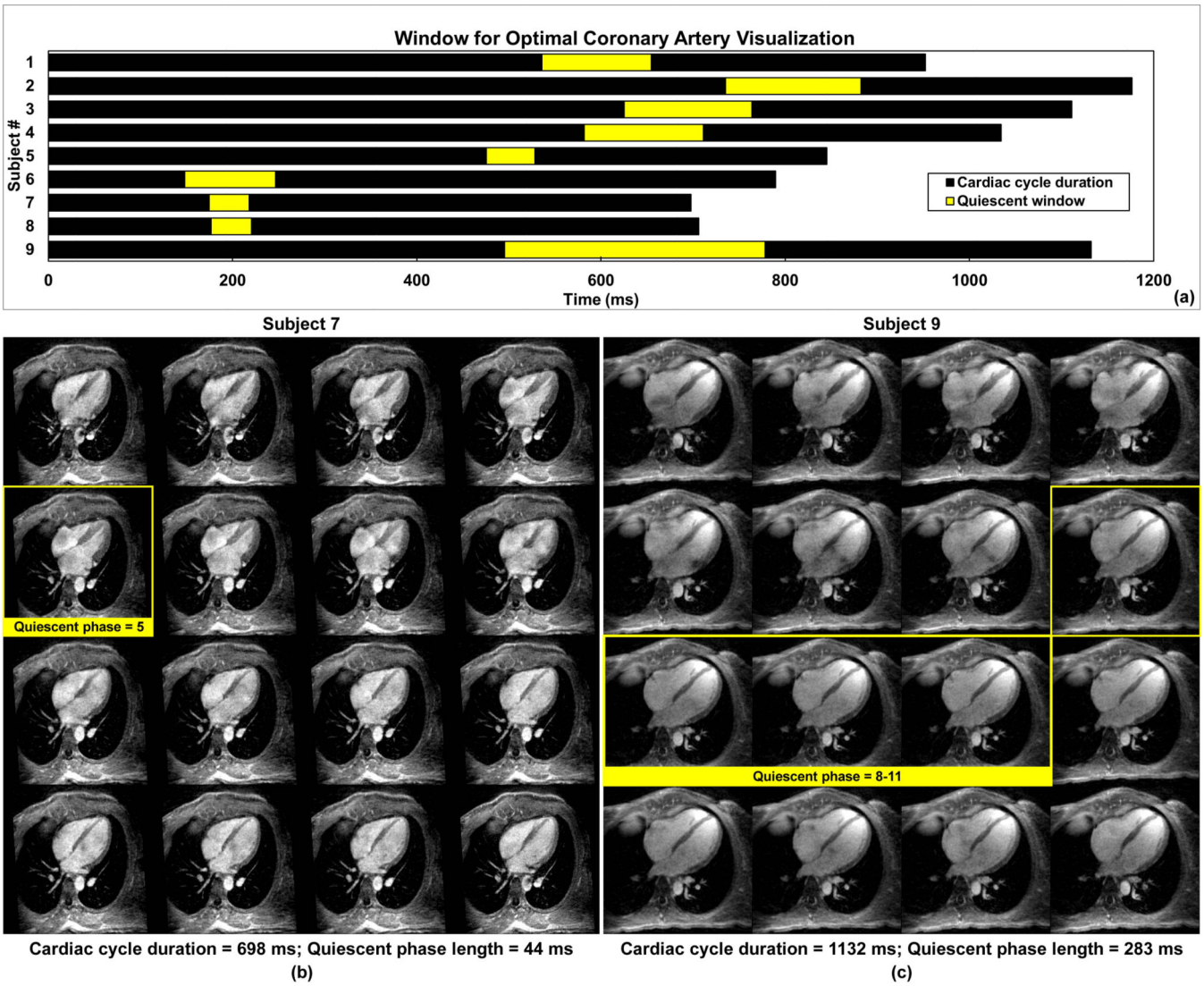

Figure 5.

The cardiac cycle durations (total length of the bars) and the quiescent periods (highlighted portions) of all 9 subjects are shown in (a). For subjects with higher heart rates (subject 6–8; 76–86 bpm), the peak-systole phase usually yields the least coronary motion, as opposed to the mid-diastole phase for the other subjects (subject 1–5, 9; 51–71 bpm). Shown in (b) are the 16 cardiac phases of subject 7 in four-chamber view reformatted from the 3D whole-heart volume. The window with the best coronary artery visualization contains phase 5. Shown in (c) are the 16 cardiac phases of subject 9 in four-chamber view reformatted from the 3D whole-heart volume. The window with the best coronary artery visualization contains phase 8–11.

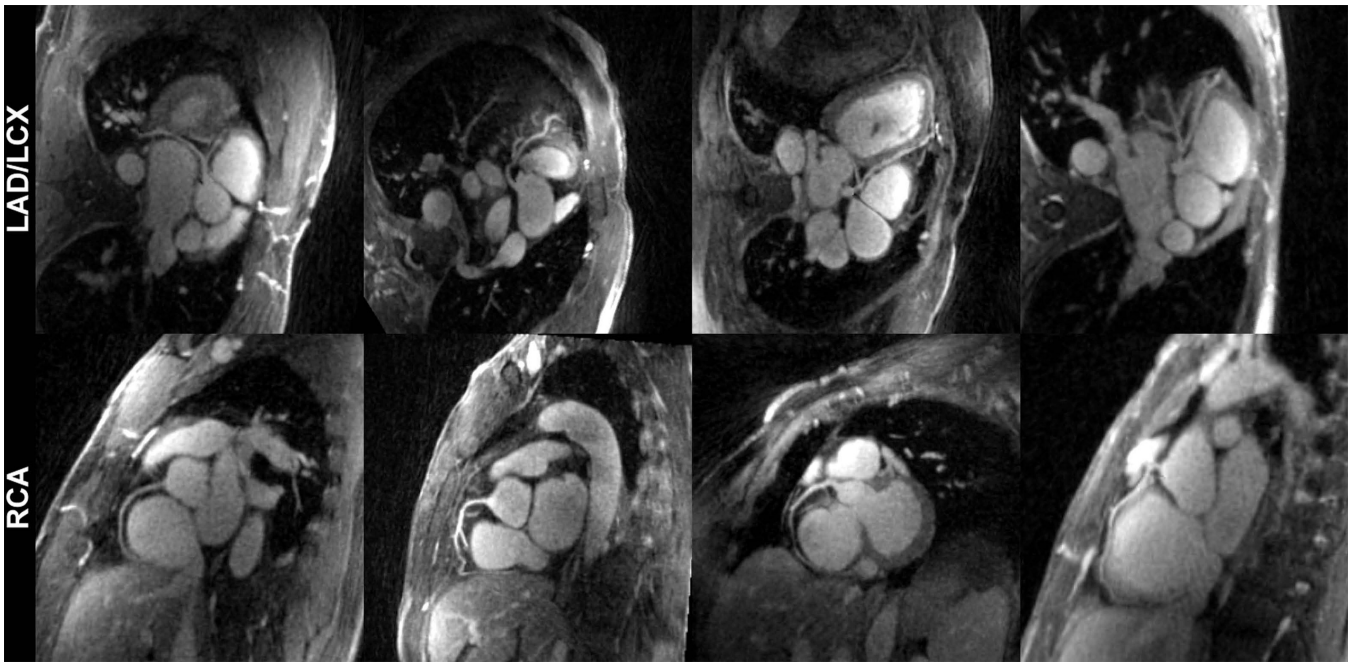

Figure 6.
Reformatted quiescent phase images from 4 example subjects showed excellent depiction of the major coronary branches.

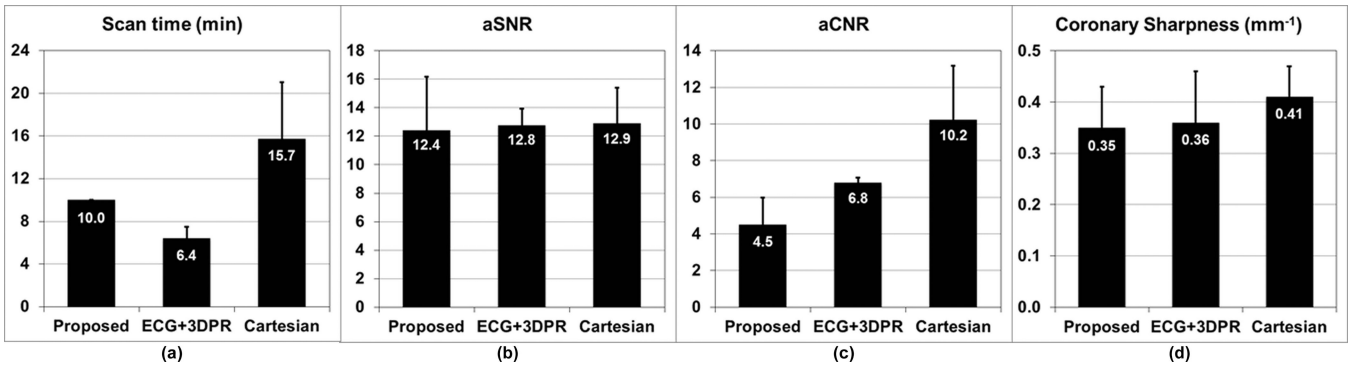

Figure 7.

Comparing the three coronary MRA protocols in terms of scan time, aSNR, aCNR and coronary sharpness. (a) while the proposed method offered a fixed 10-min scan time, the scan time of ECG+3DPR depended on the subject's heart rate, and the scan time of Cartesian depended on the subject's heart rate as well as breathing pattern; (b) the three techniques provided similar aSNR; (c) the aCNR of the proposed method, which depended on the steady-state T1 weighting, was lower than those of the other two IR-prepared techniques; (d) the coronary sharpness was comparable for the three techniques.

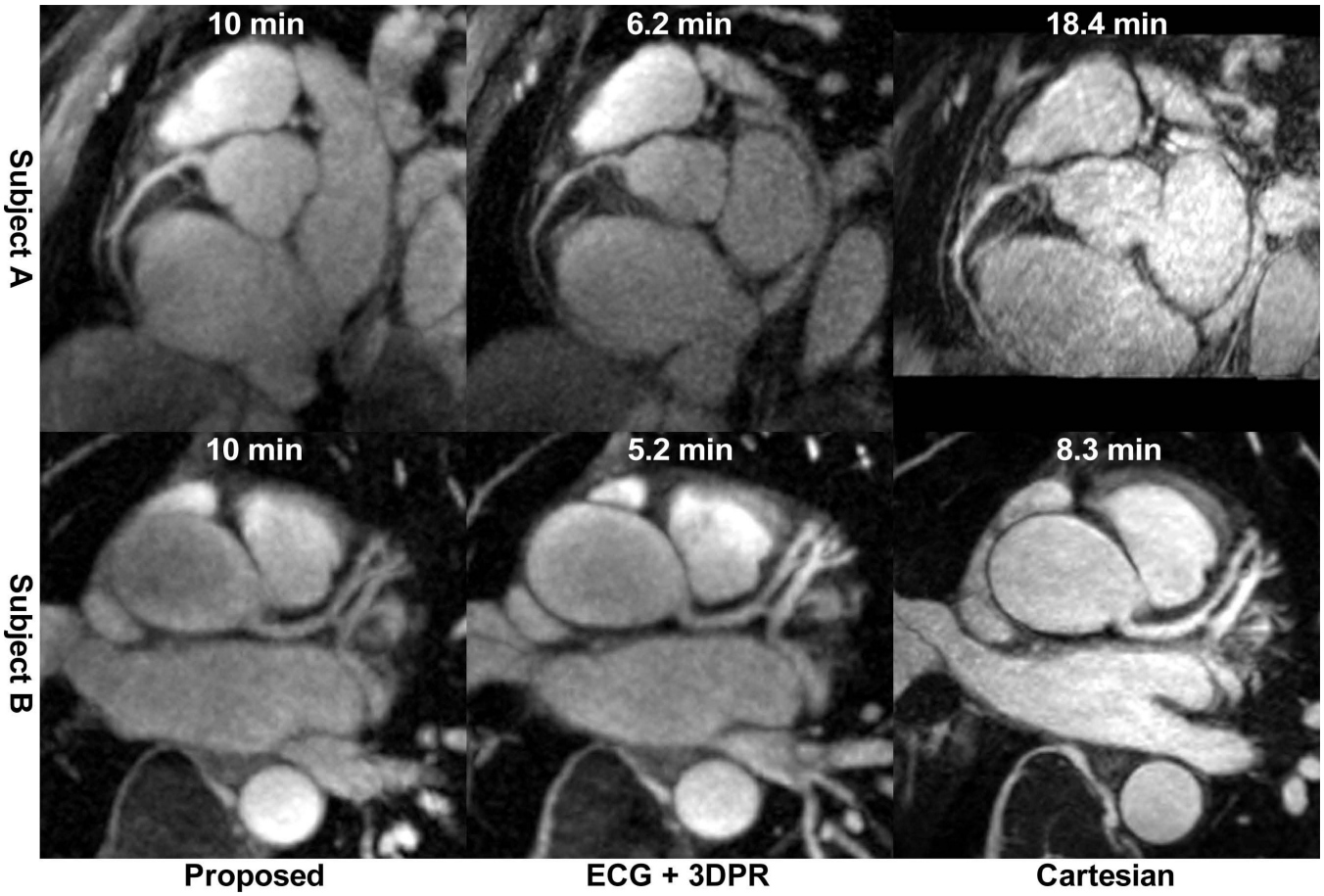

Figure 8.
Example images from the three coronary MRA techniques of two subjects. Also shown is the scan time for each image.